

Received March 1, 2020, accepted March 17, 2020, date of publication March 23, 2020, date of current version April 1, 2020.

Digital Object Identifier 10.1109/ACCESS.2020.2982487

Hybrid Active Contour Based on Local and Global Statistics Parameterized by Weight Coefficients for Inhomogeneous Image Segmentation

ASIM NIAZ¹, KAYNAT RANA², ADITI JOSHI¹, ASAD MUNIR³, DAEUN DANA KIM¹,
HYUN CHUL SONG¹, AND KWANG NAM CHOI¹

¹Department of Computer Science and Engineering, Chung-Ang University, Seoul 06974, South Korea

²Department of Electrical Engineering, University of Engineering and Technology, Taxila 47080, Pakistan

³Department of Industrial and Information Engineering, Università degli Studi di Udine, 33100 Udine, Italy

Corresponding author: Kwang Nam Choi (knchoi@cau.ac.kr)

This work was supported in part by the National Research Foundation of Korea (NRF) grant funded by the Korea government Ministry of Science and Information Technology (MSIT) under Grant 2019R1F1A1062612, and in part by the Chung-Ang University Research Scholarship Grants in 2018.

ABSTRACT Image inhomogeneity often occurs in real-world images and may present considerable difficulties during image segmentation. Therefore, this paper presents a new approach for the segmentation of inhomogeneous images. The proposed hybrid active contour model is formulated by combining the statistical information of both the local and global region-based energy fitting models. The inclusion of the local region-based energy fitting model assists in extracting the inhomogeneous intensity regions, whereas the curve evolution over the homogeneous regions is accelerated by including the global region-based model in the proposed method. Both the local and global region-based energy functions in the proposed model drag contours toward the accurate object boundaries with precision. Each of the local and global region-based parts are parameterized with weight coefficients, based on image complexity, to modulate two parts. The proposed hybrid model is strongly capable of detecting region of interests (ROIs) in the presence of complex object boundaries and noise, as its local region-based part comprises bias field. Moreover, the proposed method includes a new bias field (NBF) initialization and eliminates the dependence over the initial contour position. Experimental results on synthetic and real-world images, produced by the proposed model, and comparative analysis with previous state-of-the-art methods confirm its superior performance in terms of both time efficiency and segmentation accuracy.

INDEX TERMS Active contours, bias field, image segmentation, intensity inhomogeneity, level set.

I. INTRODUCTION

Image segmentation continues to be one of the basic and crucial problems in image processing and computer vision [1]. Object detection, object recognition, and image analysis are among the applications of image segmentation [2]–[4]. The purpose of image segmentation is to distinguish between the objects of interest and the background in an image. The object or region of interest is classified based on certain characteristics such as intensity, texture, or color [5]. There are certain factors that may affect the segmentation process, e.g., noise, low contrast, and sudden intensity variations. This sudden intensity variation is termed as image inhomogeneity

and is most likely to occur in real-world images. Image inhomogeneity mostly occurs due to the spatial variations caused by the defects in the imaging devices or modalities. Fig. 1 represents examples of homogeneous, and inhomogeneous images.

Different algorithms have been proposed based on the segmentation applications and image types [3]. There are three different types of image segmentation methods: thresholding-based, supervised-based, and unsupervised-based methods. Deep learning-based image segmentation methods belong to the supervised method category, and require large resources and datasets as compared to other methods [47]. Active contour model (ACM) is one of the most popularly used unsupervised segmentation methods over the last two decades. It was originally proposed by Kass *et al.* as an effective

The associate editor coordinating the review of this manuscript and approving it for publication was Jun Wang.

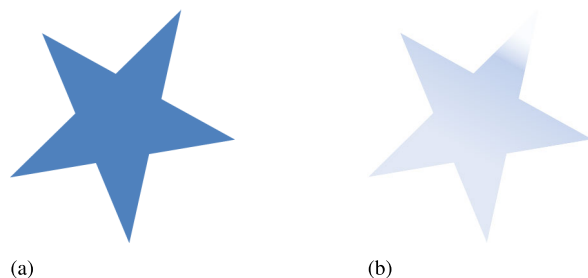


FIGURE 1. Example images: a. Homogeneous image, b. Inhomogeneous image.

method to obtain smooth closed boundaries around the object of interest [6]. Since then, active contours are being used in the area of image segmentation. The working principle of ACM is to evolve a planar curve, defined by the level set function termed as snake, under two main constraints: external and internal energies. Both the external and internal energies evolve under partial differential equations and become zero at the object boundaries [7]. The ACM energy formulation depends on the image type and, therefore, can be classified into two different types: Edge-based ACMs [8]–[13] and Region-based ACMs [14]–[30].

Edge-based ACMs adopt image gradient data which are used to form a balloon force. This balloon force pulls the internal and external energies to the object boundaries, producing segmentation results. Though the edge-based models are very strong in terms of detecting distinct objects, they are exceptionally delicate to noise interference and fail to capture weak or blurred edges in images. On the contrary, region-based ACMs adopt statistical information from inside and outside the contour and perform accurate segmentation over fuzzy regions as well. In classic region-based methods, it is assumed that the region-of-interest (ROI) comprises only homogeneous intensities, which renders them incapable of capturing obscure image boundaries.

Region-based methods are further classified into two categories: local region-based (LR) [16]–[20], [39]–[40] and global region-based (GR) methods [14], [15], [25]. The most classic global region-based method, which is based on the Mumford-Shah (M-S) model [31], was proposed by Chan and Vese by transforming the minimization problem into a mean-curvature-flow problem [25]. It can segment homogeneous images; however, it fails to effectively capture the ROIs in inhomogeneous images. To resolve this poor performance problem over inhomogeneous images, Li *et al.* proposed the Local Binary Fitting (LBF) model [14], [43], which utilizes the local image information. Though this method yields satisfactory results for the segmentation of inhomogeneous images, it heavily depends on the initial contour position. Carrying on this local image information idea, Zhang *et al.* proposed the Local Image Fitting (LIF) model to map the input image domain, by using a sliding window method, to another domain [20]. In the LIF method, Gaussian kernel is used to keep the level set regularized during evolutions.

Although GR methods are generally preferred over LR methods for their robustness, they cannot extract accurate local statistical information from inhomogeneous images [14]–[20], [25]. Therefore, ACMs consisting of multiple object features provide a better segmentation accuracy than either LR or GR alone in images with intensity variations [32]. Intensity inhomogeneity in images is assumed by the estimation of bias field. Bias field is the region responsible for intensity inhomogeneities in images; various techniques have been proposed to estimate the bias field [33]–[38]. Zhang *et al.* in [34], [35] presented their LR models to segment the inhomogeneous images by estimating the bias field. In [34] a variational level set bias correction (VLSBC) model was presented for the simultaneous segmentation and bias field estimation of inhomogeneous images. The limitation of this model is its dependence on the position of the initial contour.

Fig. 2 shows the segmentation result of a white-background image with an inhomogeneous object. It can be deduced from this figure that the LR methods are capable of handling inhomogeneous images more effectively as compared to the GR methods.

This research aims to contribute to the unsupervised methods literature in the ACMs category. of the image segmentation methods. The main contributions of our research are summarized as:

- Based on the LR and GR model analysis, this study presents a hybrid active contour model comprising both the LR and GR features to confine the contours to the exact object boundaries.
- The inclusion of LR ACM features assists the contour to capture the inhomogeneous ROIs, while the GR ACM features accelerate the robust contour evolution over the homogeneous regions.
- The LR method, in the proposed model, is incorporated with the bias field to enhance the segmentation accuracy over the inhomogeneous regions making it robust to noise.
- Each of the LR and GR parts are parametrized with weights, based on the image complexity, to modulate the two parts. This modulation contributes to parametrize the statistical information of both the LR and GR parts.
- The proposed method, includes a new bias field (NBF) initialization making the proposed model independent of the initial contour position.

After the implementation of the proposed hybrid active contour model, we performed contour evolution over synthetic and real images. Experimental results and analysis confirm the efficiency of the proposed method over state-of-the-art methods in comparison.

The remaining sections of this paper are categorized as follows. Section II covers the related works, and Section III describes the proposed methodology. Section IV presents the results of the proposed method in comparison to previous methods. Section V describes the segmentation accuracy

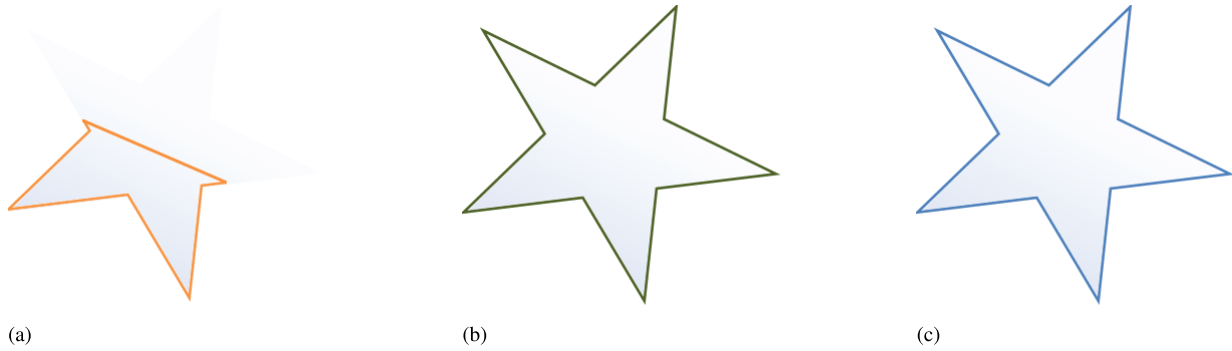


FIGURE 2. Segmentation of images with white background and intensity of an inhomogeneous object: a. C-V method, b. LBF method, and c. LIF method.

using the Noise Sensitivity Evaluation method and quantitative comparison. Section VI presents Discussion. Finally, the concluding statements are summarized in Section VII.

II. RELATED WORKS

A. MUMFORD-SHAH (M-S) MODEL

The Mumford-Shah (M-S) model [31] is the most famous and basic region-based image segmentation method; it restricts the energy function to an optimal approximation function $u(x)$ which changes smoothly within a sub region of the given image $I(x)$.

Let $I(x) : \Omega \rightarrow R$ be a given gray level image with a domain of definition Ω and $u(x)$ the image’s model: the M-S functional is defined as

$$F_{MS}(I, C) = \lambda \int_{\Omega} (I(x) - u(x))^2 dx + v \int_{\Omega \setminus C} (\nabla u(x))^2 dx + \mu \int_{\Omega} Length(C), \quad (1)$$

where μ and v are related coefficients with positive values; C is a closed set made up of singular points joined by smooth arcs meeting only at end points. $Length(C)$ is the total length of the curve making contour C . The M-S functional was proposed to establish an optimal criterion for segmenting an image into sub-regions.

The M-S model shows non-regularity of the edge term and non-convex performance, creating trouble through energy minimization process.

B. CHAN-VESE (CV) MODEL

The C-V model [25] is based on the Mumford-Shah functional [31] and was proposed by Chan and Vese to detect objects in a given image. The C-V model is based on the curve evolution technique of ACMs. This model assumes that the image consists of homogeneous intensity regions. Let $\Omega \subset R^2$ be the image domain, and $I(x) : \Omega \rightarrow R^2$ is the given gray level image with pixel x , given that $C : [0, 1] \rightarrow R^2$ be a closed, arbitrary curve. This curve C divides the image into two non-overlapping regions: the inside region C_{in} and the outside region C_{out} . The external energy function of C-V

model is proposed as:

$$F_{CV}(C, a_1, a_2) = \lambda_1 \int_{outside(C)} |I(x) - a_1|^2 H_{\epsilon}(\phi(x)) dx + \lambda_2 \int_{inside(C)} |I(x) - a_2|^2 (1 - H_{\epsilon}(\phi(x))) dx + \mu \int_{\Omega} |\nabla H_{\epsilon}(\phi(x))|^2 dx + v \int_{\Omega} H_{\epsilon}(\phi(x)) dx, \quad (2)$$

where $outside(C)$ and $inside(C)$ are the regions outside and inside the contour C , respectively. a_1 and a_2 are two constants to approximate the average of the inner and outer region intensities, respectively. λ_1, λ_2 , and μ are three constants with values ≥ 0 , whereas ϵ represents a correspondent coefficient. H_{ϵ} stands for the Heaviside function, defined as

$$H_{\epsilon}(\phi(x)) = \frac{1}{2} \left(1 + \frac{2}{\pi} \arctan \left(\frac{\phi}{\epsilon} \right) \right). \quad (3)$$

a_1 and a_2 are equal to

$$a_1 = \frac{\int_{\Omega} I(x) H_{\epsilon}(\phi(x)) dx}{\int_{\Omega} H_{\epsilon}(\phi(x)) dx}, \quad a_2 = \frac{\int_{\Omega} I(x) (1 - H_{\epsilon}(\phi(x))) dx}{\int_{\Omega} (1 - H_{\epsilon}(\phi(x))) dx}. \quad (4)$$

Keeping a_1 and a_2 fixed, (2) is minimized using the gradient descent algorithm [42] as

$$\frac{\partial \phi}{\partial t} = -\lambda_1 \delta_{\epsilon}(\phi) (I - a_1)^2 + \lambda_2 \delta_{\epsilon}(\phi) (I - a_2)^2 + \mu \delta_{\epsilon}(\phi) \operatorname{div} \left(\frac{\nabla \phi}{|\nabla \phi|} \right) - v \delta_{\epsilon}(\phi), \quad (5)$$

where $\delta_{\epsilon}(x)$ is the Dirac delta function, defined as

$$\delta_{\epsilon}(\phi) = \frac{\epsilon}{\pi(\phi^2 + \epsilon^2)} \quad (6)$$

The width of the $\delta_{\epsilon}(x)$ function is controlled by the parameter ϵ in (2). The C-V model is a powerful method to segment many types of images which are quite difficult to segment using gradient based or thresholding techniques. This model works under the assumption that the input image has homogeneous intensities, therefore, the model works well on homogeneous images. However, for inhomogeneous images, it leads to a poor performance.

C. LOCAL BINARY FITTING (LBF) MODEL

Huang and Zeng [14], [43] presented their Local Binary Fitting (LBF) model by embedding local image information to deal with intensity inhomogeneous images. The core idea of LBF is to define its energy function by introducing a Gaussian kernel function.

$$K_\sigma(x - y) = \frac{1}{(2\pi)^2 \sigma^n} \exp\left(-\frac{|x - y|^2}{2\sigma^2}\right) \quad (7)$$

stands for a Gaussian kernel (window function); its standard deviation, to balance localization, is represented by σ . The LBF energy function is defined as

$$\begin{aligned} F_{LBF}(C, f_1, f_2) &= \lambda_1 \int_{\Omega} K_\sigma(x - y) |I(y) - f_1(x)|^2 H_\epsilon(\phi(y)) dy \\ &+ \lambda_2 \int_{\Omega} K_\sigma(x - y) |I(y) - f_2(x)|^2 (1 - H_\epsilon(\phi(y))) dy \\ &+ \mu \int_{\Omega} \frac{1}{2} (\nabla\phi(x) - 1)^2 dx + \nu \int_{\Omega} \delta_\epsilon(\phi(x)) |\nabla\phi(x)| dx, \end{aligned} \quad (8)$$

where λ_1 and λ_2 are the scaling coefficients with values ≥ 0 . $H_\epsilon(\phi)$ and $\delta_\epsilon(\phi(x))$ are the Heaviside function and Dirac delta function as defined by (3) and (6). The inclusion of K_σ scans an image's local intensity statistical information within both sides of the curve C ; it assists the LBF model to capture the inhomogeneous ROIs.

$$f_1(x) = \frac{K_\sigma * [H_\epsilon(\phi)I(x)]}{K_\sigma * H_\epsilon(\phi)} \quad (9)$$

and

$$f_2(x) = \frac{K_\sigma * [(1 - H_\epsilon(\phi))I(x)]}{K_\sigma * (1 - H_\epsilon(\phi))} \quad (10)$$

represent the local intensity means inside and outside the curve C , respectively, and are computed as local neighborhood. A stable outcome is guaranteed with the incorporation of the distance regularization term from [44] into (8). The LBF energy function from (8) is minimized as

$$\begin{aligned} \frac{\partial\phi}{\partial t} &= -\lambda_1 \delta_\epsilon(\phi) \int_{\Omega} K_\sigma(x - y) |I(x) - f_1(y)|^2 dx \\ &+ \lambda_2 \delta_\epsilon(\phi) \int_{\Omega} K_\sigma(x - y) |I(x) - f_2(y)|^2 dx \\ &+ \nu \delta_\epsilon \operatorname{div} \left(\frac{\nabla\phi}{|\nabla\phi|} \right) + \mu \left(\nabla\phi - \operatorname{div} \left(\frac{\nabla\phi}{|\nabla\phi|} \right) \right), \end{aligned} \quad (11)$$

where μ is a constant coefficient that serves to initiate the curve movement towards the object boundaries. The drawback of this method is its potential vulnerability to stuck in a local minima. Therefore, this dependence on the initial contour position sometimes degrades the efficiency of the LBF model.

D. LOCAL IMAGE FITTING (LIF) MODEL

Zhang *et al.* proposed the Local Image Fitting (LIF) model by introducing LIF energy for the segmentation of images that were affected by inhomogeneity [20]. The working principle of this model is the calculation and minimization of the distance between the fitted and original images as

$$F_{LIF} = \frac{1}{2} \int_{\Omega} |I(x) - I_{LIF}(x)|^2 dx \quad (12)$$

I_{LIF} in (12) is the local fitted image, defined as

$$I_{LIF}(x) = f_1(x)H_\epsilon(\phi) + f_2(x)(1 - H_\epsilon(\phi)), \quad (13)$$

where $f_1(x)$ and $f_2(x)$ are the local intensity means in the given image defined in (9) and (10), respectively. Utilizing the gradient descent algorithm from [42], (12) minimizes to

$$\frac{\partial\phi}{\partial t} = (I(x) - I_{LIF}(x)) (f_1(x) + f_2(x)) \delta_\epsilon(\phi), \quad (14)$$

where $f_1(x)$ and $f_2(x)$ represent local intensity means defined in (9) and (10), respectively. δ_ϵ is the Dirac delta function defined in (6). Although the LIF model is computationally less complex than the LBF model, it produces almost the similar segmentation results.

E. VARIATIONAL LEVEL SET WITH BIAS CORRECTION (VLSBC) MODEL

Zhang *et al.* [34] proposed a variational level set with bias correction (VLSBC) model for the detection and segmentation of corrupted images with inhomogeneous intensities. The VLSBC model computes the bias field, which is responsible for the intensity inhomogeneity in an image, and keeps the contour evolution smooth over the data term. A local clustering criterion function, first, drives the local clustering to capture the neighboring intensities around each point. The VLSBC model depends on the retinex image model to demonstrate images as $I(x) = b(x)J(x) + n(x)$, where $I(x)$ and $b(x)$ represent the original image and bias field, respectively. $J(x)$ is the true image, independent of intensity inhomogeneity, whereas $n(x)$ is the additive noise in original image. The true image, $J(x)$, concept is mathematically visualized as

$$J(x) \approx \sum_{i=1}^N m_i M_i(\phi), \quad (15)$$

where m_i represents the intensity means for distinct regions ω_i , and $i = 1, 2, 3, \dots, i$. The local clustering criterion function is based on the iterative k-means algorithm to minimize the energy function,

$$E \approx \int \left(\sum_{i=1}^N \int_{\Omega_i} K_\sigma(x - y) |I(y) - b(x)m_i|^2 dy \right) dx. \quad (16)$$

The energy function is further minimized as

$$E = \int \left(\sum_{i=1}^N \int_{\Omega_i} K_\sigma(x - y) |I(y) - b(x)m_i|^2 M_i(\phi) dy \right) dx, \quad (17)$$

where M_i is the membership function of the associated regions with $x \in \{\Omega_i\}_{i=1}^N$. In (17), $b(x)$ and the intensity means, m_i are defined as

$$b(x) = \frac{\sum_{i=1}^N K_\sigma * (I(x)m_i M_i(\phi))}{K_\sigma * (m_i^2 M_i(\phi))} \quad (18)$$

$$m_i = \frac{\int K_\sigma * (I(x)b(x)M_i(\phi))}{K_\sigma * (b(x)^2 M_i(\phi))} \quad (19)$$

VLSBC is a robust method for the segmentation of inhomogeneous images. However, it has limitation in terms of initial contour dependence.

F. NEW BIAS FIELD (NBF) INITIALIZATION

The VLSBC model initializes the bias field from $b(x) = 1$ for $x \in \Omega$ in the first iteration. This initialization may cause the zero-level set to be far away from the object boundaries for next iterations, leading to false bias field estimation. This incorrect bias field estimation may result in inaccurate segmentation results. To overcome this shortcoming, Huang, Ji, and Zhang formulated a new bias field initialization and assumed that the bias field varies slowly within the image domain, Ω [41]. The initialization of the new bias field is $b_0 = K_\sigma \left(\frac{I}{N_0} \right)$.

N_0 is the average of image intensities and K_σ is a Gaussian kernel, responsible for the smooth contour evolution. The restored image, J_0 , is expressed as

$$J_0 = \frac{I}{b_0} = N_0 \left(\frac{I}{K_\sigma * I} \right) \quad (20)$$

The new bias field initialization ensures the independence of the following relation from the initial contour position

$$N_0 \approx \frac{1}{2}(c_1 + c_2) \quad (21)$$

Therefore, the new bias field initialization, b_0 , allows this model to be independent of the contour initialization.

III. PROPOSED METHODOLOGY

For the segmentation of intensity inhomogeneous images, the following energy function is proposed:

$$F_{proposed} = F_{hybrid} + \nu A(\phi), \quad (22)$$

where F_{hybrid} is a hybrid energy function that comprises the global-based and local-based energy fitting models; this function is defined later in the paper. $A(\phi)$ represents the area term used to speed up the contour evolution process; ν is a positive coefficient to penalize the area term. The following relation defines the area term:

$$A(\phi) = \int H_\epsilon(\phi) \quad (23)$$

In (22), F_{hybrid} is an externally proposed incremental energy function; it contributes to an accurate contour fitting in inhomogeneous images and reduces the time complexity of contour evolution. F_{hybrid} is defined as:

$$F_{hybrid}(\phi) = \int_{\Omega} \frac{w}{(1-w)} (I - I_{bLFI}) dx$$

$$+ \int_{\Omega} \frac{w}{(1-w)} ((I - I_{GFI})) dx \quad (24)$$

In (24), I_{bLFI} and I_{GFI} are the local and global fitted models, respectively; both the models are defined as:

$$I_{bLFI} = b(x)(m_1 M_1 + m_2 M_2), \quad (25)$$

$$I_{GFI} = a_1 M_1 + a_2 M_2, \quad (26)$$

where m_1 and m_2 are the local intensity means whereas a_1 and a_2 are the global intensity means defined in VLSBC and, CV respectively. M_1 and M_2 are the membership functions with values

$$M_1 = H_\epsilon(\phi) \quad (27)$$

and

$$M_2 = (1 - H_\epsilon(\phi)), \quad (28)$$

respectively.

The component $b(x)$ represents the bias field, responsible for the intensity variations in images. $b(x)$ is incorporated with the local fitted model to increase its performance while segmenting the inhomogeneous regions.

w is a scaling parameter inspired from [47], $w = \text{average}(C_N) \cdot (1 - C_N)$; C_N reflects how rapidly intensity changes within the local window of size N , defined as $C_N = \frac{I_g - I_{min}}{I_{max} - I_{min}}$. Both w and $(1 - w)$ have values between 0 and 1. I_{min} , I_{max} are the minimum and the maximum of intensity within that local window, respectively. I_g represents the intensity level of image that is usually 255. The value of w is based on the degree of image inhomogeneity, where a higher value implies a higher degree of inhomogeneity and vice versa.

Global energy fitting models are designed under a general assumption that the images contain homogeneous intensities only and, therefore, they are insufficient to capture the objects of interest in inhomogeneous images. On the other hand, though local energy fitting models can handle inhomogeneous images, they are complex in terms of time efficiency. Therefore, both the models have their tradeoffs.

It is a general assumption that the intensity inhomogeneity itself is a smoothly varying function that affects the image intensities. The VLSBC [34] model assumes inhomogeneity as multiplicative or additive in nature. Suppose $I : \Omega \rightarrow R^2$ is an input image that is affected by intensity inhomogeneity; $J(x)$ is the true image, independent of inhomogeneity. For a partition of the image domain, $\{\Omega_i\}_{i=1}^N$, $J(x)$ takes N distinct constant values c_1, \dots, c_N in disjoint regions $\Omega_1, \dots, \Omega_N$, respectively. The bias field, $b(x)$, varies slowly and can be approximated with a Gaussian distribution and additive noise, $n(x)$. This multiplicative estimation model is defined as:

$$I = b(x)J(x) + n(x). \quad (29)$$

If the additive noise is set to be 0, then the true image $J(x)$ can be obtained as:

$$J(x) = \frac{I}{b(x)}. \quad (30)$$

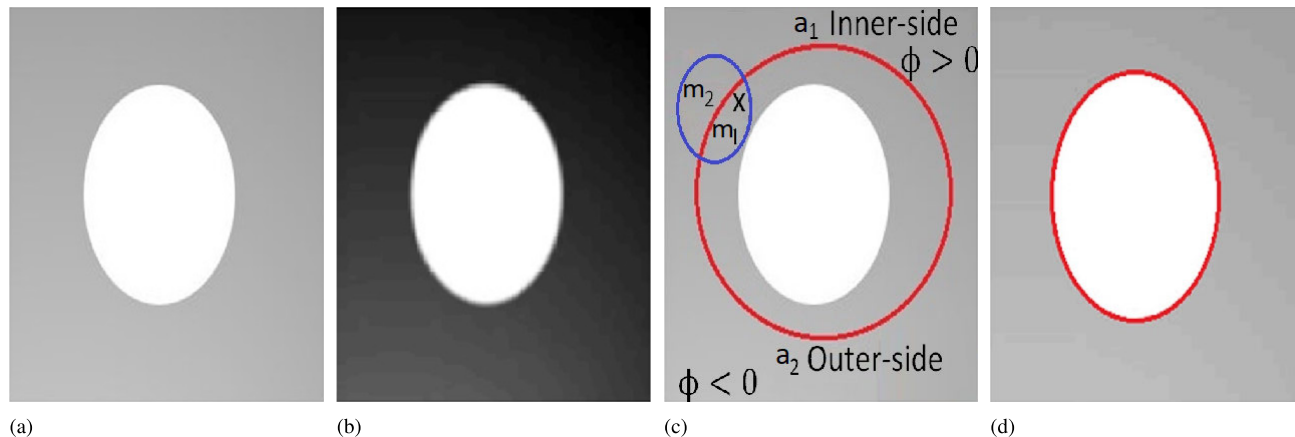


FIGURE 3. Graphical representation of the proposed model: a. original input image, b. bias field estimation, c: level set evolution, d. segmentation result.

The image inhomogeneity degree can be modeled from (29) as:

$$I = b \sum_{i=1}^N m_i M_i, \quad (31)$$

where M_i represents the membership function associated to each of the regions from $\{\Omega_i\}_{i=1}^N$. The bias field is dependent on the initial position of the contour. Therefore, to make it independent of the initial position, the new bias field initialization is used from [41] as:

$$b_0 = K_\sigma \left(\frac{I}{N_0} \right), \quad (32)$$

where b_0 represents the new bias field initialization, K_σ represents the Gaussian kernel, and N_0 accounts for the average of image intensities.

A curve C , defined as level set function ϕ , which is zero $\phi = 0$ at the object boundary divides image into two region: inside and outside. According to the calculus of variation, the gradient descent algorithm [42] parameterizes (1) as:

$$\left(\frac{w}{1-w} \right) b(x) \delta(\phi) (m_1 + m_2) (I(x) - I_{LIF}) - v \delta(\phi) + \left(\frac{w}{1-w} \right) \delta(\phi) (I(x) - I_{GFI}) (a_1 + a_2), \quad (33)$$

where a_1 , a_2 and m_1 , m_2 are acquired from (4) and (19), respectively.

The visual representation of the proposed model is shown in Fig. 3, which represents the local and global statistical information utilization in the proposed model. The derived near-optimal parameter settings are represented in Table 1.

The level set function of the proposed model is initialized as

$$\phi_{t=0} = \begin{cases} -p, & x \in \Omega_0 - \partial\Omega_0 \\ 0, & x \in \partial\Omega_0 \\ p, & x \in \Omega - \Omega_0. \end{cases} \quad (34)$$

In (34), p is a constant parameter, Ω_0 is a subset of the image domain Ω , and $\partial\Omega_0$ is the boundary of Ω_0 .

TABLE 1. Parameter settings.

Parameter	Name	Value
Δt	Time step	0.01
p	Initial level set	2
σ	Gaussian kernel	2.5
v	Area penalization term	$0.00001 * 255 * 255$
w	Weight coefficient	(0, 1)

Algorithm 1 Iterative Algorithm for the Proposed Model

Input: The original image $I(x)$, and parameters from Table 1.

- 1) Set the new bias field initialization with (32).
- 2) **Initialize** the level set function, ϕ from $t = 0$, with (34)
- 3) Iteration count from $m = 0$.
- 4) **while** contour evolution does not converge **do**
- 5) Compute m_i , from (19).
- 5) Compute a_i , from (4).
- 6) Update bias field $b(x)$ using (18).
- 7) Solve the PDE (33) in ϕ to obtain $\phi_{(t+1)}$.
- 8) $m = m + 1$.
- 9) **End while**

Output: Final segmentation, final ϕ

A. ALGORITHM

The description of the proposed algorithm is summarized as follows:

IV. RESULTS

This section presents the performance of the proposed method against previous state-of-the-art methods. The experiment was carried out on multiple synthetic and real images. MATLAB 2018a, installed in a 64-bit OS (Windows 10) with a 3.40 GHz Intel Core i7 microprocessor and an 8 GB RAM, was used for both implementation and testing.

The proposed method is independent of the contour initialization, as shown by Fig. 4. The top row in Fig. 4 shows

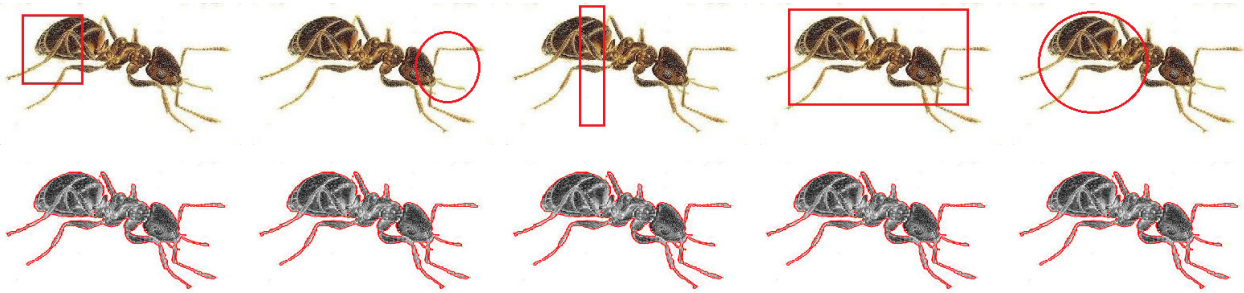


FIGURE 4. Proposed method on a synthetic image. Top row: input image with contours, of different sizes, at different locations; second row: corresponding results.

TABLE 2. CPU time and number of iterations required for segmentation results in Fig. 5.

Methods		Col 1	Col 2
C-V[25]	CPU Time (s)	1.99	5.6
	Iterations	100	500
LBF [43]	CPU Time (s)	7.45	7
	Iterations	500	500
LIF [20]	CPU Time (s)	0.92	1.96
	Iterations	80	500
VLSBC [34]	CPU Time (s)	0.99	3.43
	Iterations	7	36
Zhang et al. [35]	CPU Time (s)	3.74	4.73
	Iterations	50	50
FRAGL [48]	CPU Time (s)	1.02	1.80
	Iterations	10	50
Proposed Model	CPU Time (s)	0.91	1.39
	Iterations	2	6

the input image with initial contour at different locations, and the second row shows corresponding results. Note that the contour, with different shapes and sizes, is initialized from four different positions, producing similar type of results.

Fig. 5 is a representation of the comparison between the proposed method and other state-of-the-art methods for one object synthetic image with different inhomogeneity levels. Top row to the eighth row represent the input images and the results generated by C-V [25], LBF [43], LIF [20], VLSBS [34], Zhang *et al.* [35], FRAGL [49] and proposed method, respectively. The results show that the objects in the first column are correctly segmented using all the methods, except for the LBF method [43]. This comparison illustrates that the proposed method has a better stability and greater accuracy even for the image with higher inhomogeneity level; whereas, the accuracy of other models have significantly decreased with higher inhomogeneity level.

Table 2 presents the CPU time and number of iterations taken for the segmentation of the synthetic images in Fig. 5. Although the FRAGL [49] shows near similar time efficiency to the proposed model, it fails to capture object

TABLE 3. CPU time and number of iterations required for segmentation results in Fig. 6.

Methods		Col 1	Col 2	Col 3
CV[25]	CPU Time (s)	25	32	37.63
	Iterations	500	500	500
LBF [43]	CPU Time (s)	22	26.67	25.32
	Iterations	500	500	500
LIF [20]	CPU Time (s)	7.59	9.87	15.45
	Iterations	500	500	480
VLSBC [34]	CPU Time (s)	15.01	8.87	13.06
	Iterations	50	17	27
Zhang et al. [35]	CPU Time (s)	21.32	16.73	185.9
	Iterations	50	70	65
FRAGL [48]	CPU Time (s)	4.52	2.05	3.32
	Iterations	50	20	20
Proposed Model	CPU Time (s)	1.12	1.27	1.63
	Iterations	3	3	3

boundaries adequately. It is deduced that the proposed method successfully outclasses the previous methods in terms of stability and CPU time (sec).

Fig. 6 shows some synthetic images with multiple objects having intensity variations in the background and foreground. Top row contains original (input) images, followed by the segmentation results of C-V [25], LBF [43], LIF [20], VLSBC [34], Zhang *et al.* [35], FRAGL [49] and the proposed model, respectively. The instability of the previous methods is clearly specified, where it is unable to segment inhomogeneous regions using C-V [25]. Although, LBF [43] and LIF [20] could locate the object boundaries, they lack full accuracy, thereby producing false contours. The VLSBC [34] and FRAGL [49] models suppressed false contours appearances; however, both still missed the exact object boundaries. Zhang *et al.* [35] method failed to work in the case of multiple object segmentation, whereas the proposed method achieved superior segmentation accuracy.

Table 3 presents the CPU time and number of iterations taken for the segmentation of the synthetic images in Fig. 6. Although LBF [43], LIF [20] and FRAGL [49] consumed less CPU time following the proposed method, they failed to produce an accurate segmentation. This table confirms that the proposed model, so far, outperforms the past methods.

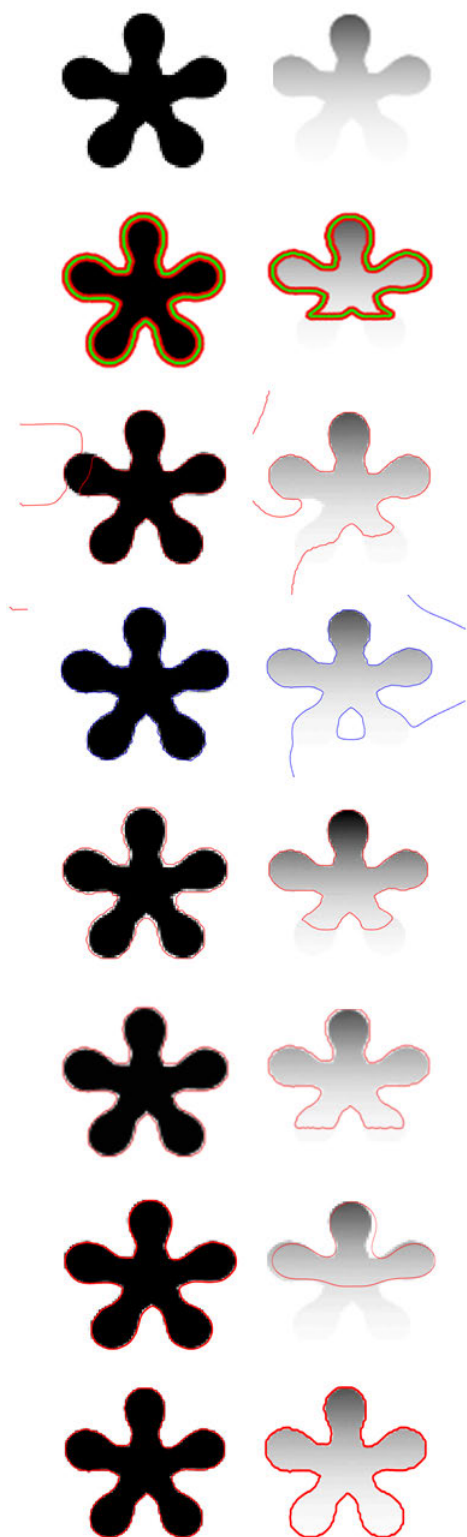


FIGURE 5. Image segmentation comparison of single-object synthetic images. Top row: Input image with different inhomogeneity levels; second row: C-V method [25]; third row: LBF method [43]; forth row: LIF method [20]; fifth row: VLSBC method [34]; sixth row: Zhang et al. method [35]; seventh row: FRAGL method [48]; eighth row: proposed method.

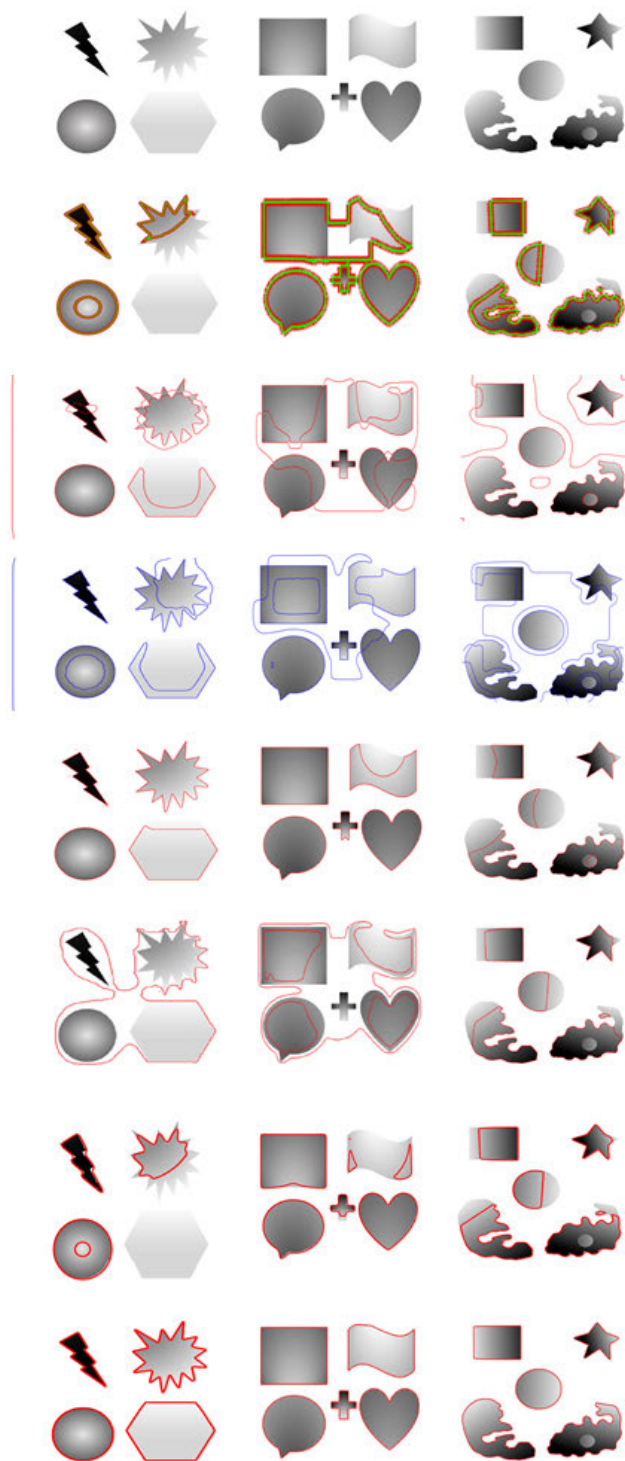


FIGURE 6. Image segmentation comparison of multiple intensity objects of synthetic images. Top row: Input images; second row: C-V method [25]; third row: LBF method [43]; forth row: LIF method [20]; fifth row: VLSBC method [34]; sixth row: Zhang et al. method [35]; seventh row: FRAGL method [48]; eighth row: proposed method.

Fig. 7 shows the comparison of the segmentation results of real images. Top row to the eighth row represent the input images, C-V [25], LBF [43], LIF [20], VLSBC [34],

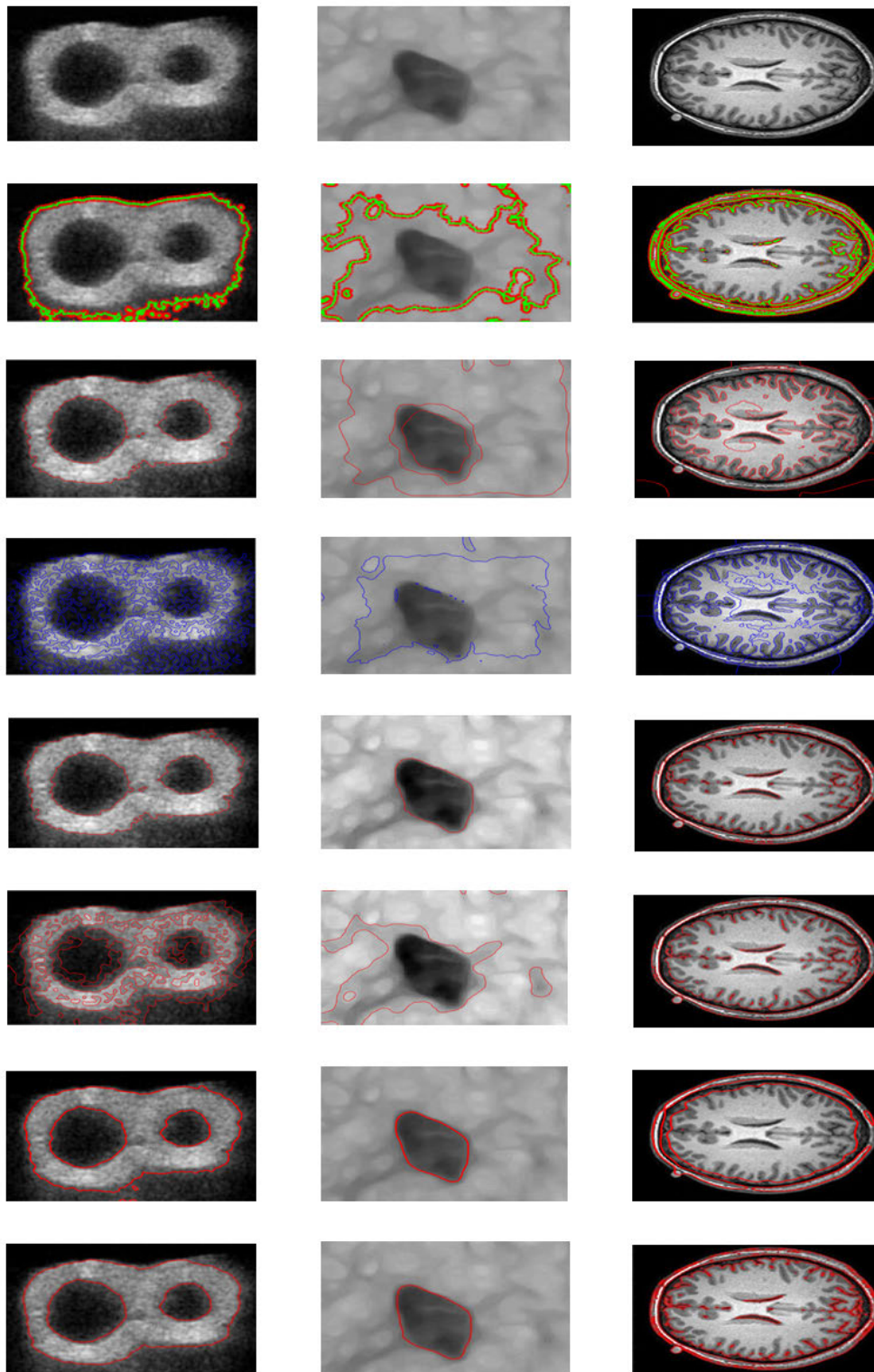


FIGURE 7. Image segmentation results of real images. Top row: Input images; second row: C-V method [25]; third row: LBF method [43]; forth row: LIF method [20]; fifth row: VLSBC method [34]; sixth row: Zhang *et al.* method [35]; seventh row: FRAGL method [48]; eighth row: proposed method.

Zhang *et al.* [35], FRAGL [48] and the proposed method, respectively. The comparison results illustrate that the LBF [43] model located the object boundaries; however,

it stimulated a false contours evolution, whereas the LIF [20] and Zhang *et al.* [35] models stuck in the local minima in this case. The FRAGL [48] showed impressive

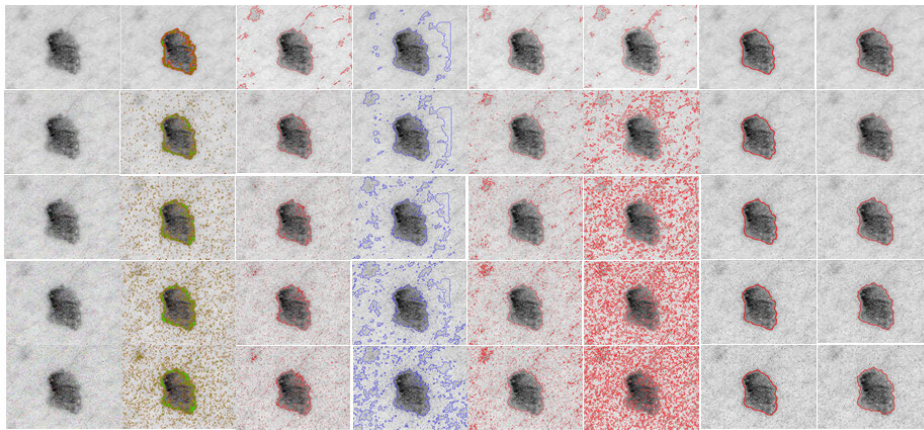


FIGURE 8. The first (left) column: Inhomogeneous images with different levels of Salt & Pepper noise: (0, 0.01, 0.02, 0.03, 0.04); the second column: C-V method [25]; the third column: LBF method [43]; the fourth column: LIF method [20]; the fifth column: VLSBC method [34]; the sixth column: Zhang et al. method [35]; the seventh column: FRAGL [48]; the eighth column: proposed method.

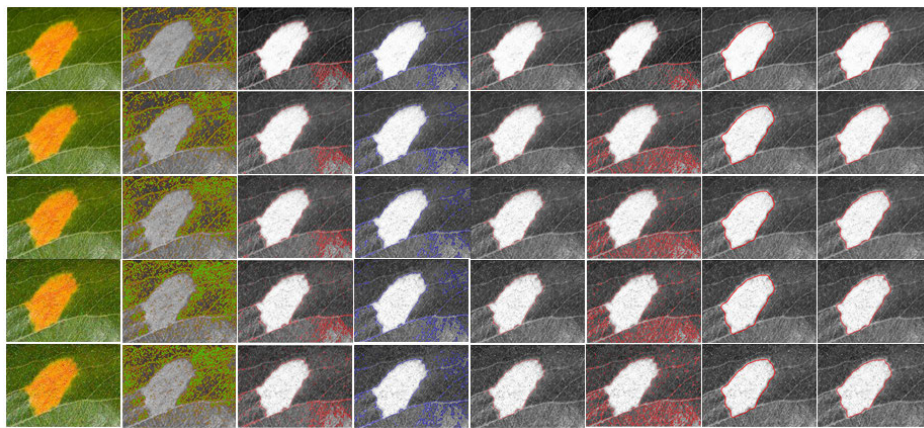


FIGURE 9. The first (left) column: Inhomogeneous images with different levels of Salt & Pepper noise: (0, 0.01, 0.02, 0.03, 0.04); the second column: C-V method [25]; the third column: LBF method [43]; the fourth column: LIF method [20]; the fifth column: VLSBC method [34]; the sixth column: Zhang et al. method [35]; the seventh column: FRAGL [48]; the eighth column: proposed method.

performance over the first two images from left, in the seventh row, but failed to segment region of interest in the third image. The VLSBC [34] model performed segmentation with a reasonable accuracy than other previous methods, whereas the proposed model surpasses all the previous methods for segmentation results.

Table 4 presents the CPU time and number of iterations taken for the segmentation of real images in Fig. 7. It is clear that, on average, the time taken by VLSBC [34], and FRAGL [48] methods are least among other models in comparison, except the proposed model.

V. SEGMENTATION ACCURACY ANALYSIS

To verify the superior performance of the proposed method over other state-of-the-art methods, a segmentation accuracy analysis was performed using two techniques, namely, the noise sensitivity evaluation and quantitative comparison.

A. NOISE SENSITIVITY EVALUATION

The NBF initialization followed by the inclusion of bias field with the LR part makes the proposed model robust to noise. To perform noise sensitivity evaluation, we used the Jaccard Similarity (JS) method. JS is used to understand the similarity between the image segmentation results. Two types of artificial noises were added to the images: Salt & Pepper and Gaussian.

The mathematical representation of the JS metric is written as

$$JS(A, B) = \frac{|A \cap B|}{|A \cup B|}, \tag{35}$$

where A and B represent the segmentation result in this experiment and the ground truths, respectively.

Figs. 8, 9 and 10 demonstrate the segmentation results of three different images with different levels of Salt & Pepper noise. From the top row to the fifth row of each of the

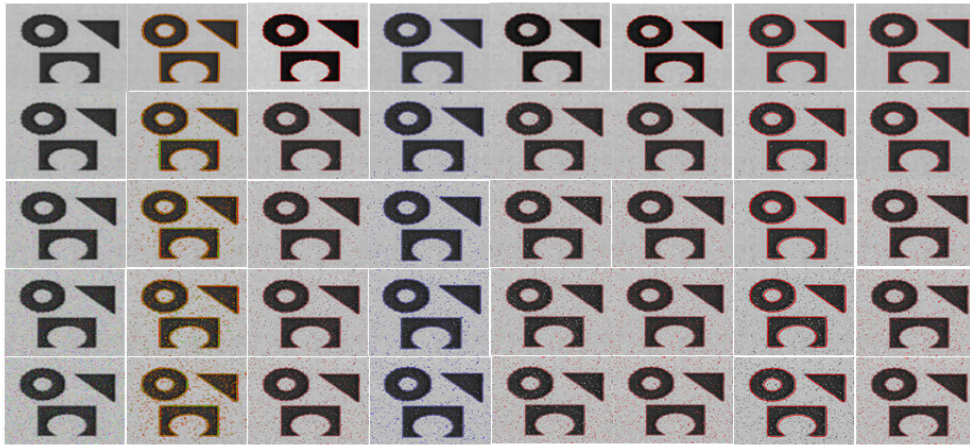


FIGURE 10. The first (left) column: Inhomogeneous images with different levels of Salt & Pepper noise: (0, 0.01, 0.02, 0.03, 0.04); the second column: C-V method [25]; the third column: LBF method [43]; the fourth column: LIF method [20]; the fifth column: VLSBC method [34]; the sixth column: Zhang *et al.* method [35]; the seventh column: FRAGL [48]; the eighth column: proposed method.

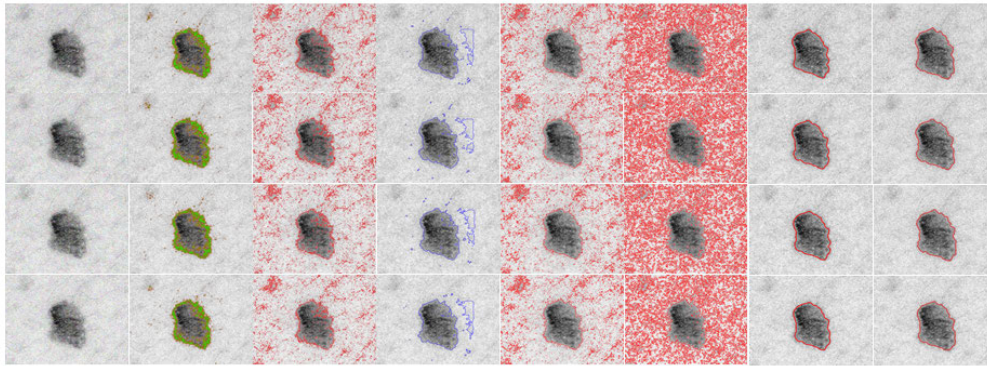


FIGURE 11. The first (left) column: Inhomogeneous images with different levels of Gaussian noise: (0.01, 0.02, 0.03, 0.04); the second column: C-V method [25]; the third column: LBF method [43]; the fourth column: LIF method [20]; the fifth column: VLSBC method [34]; the sixth column: Zhang *et al.* method [35]; the seventh column: FRAGL [48]; the eighth column: proposed method.

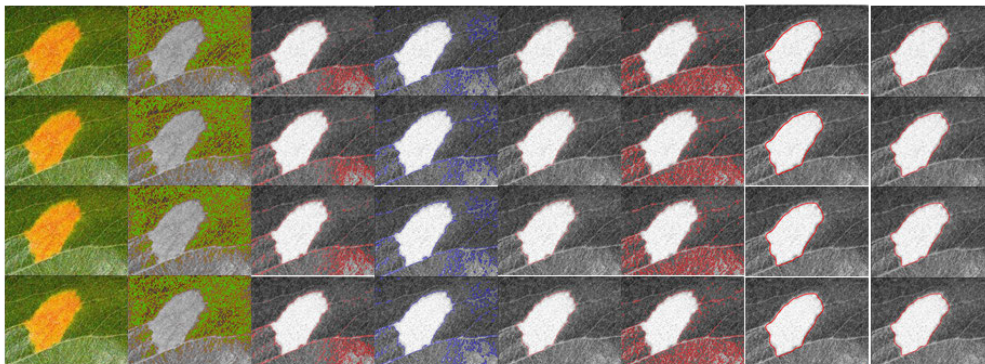


FIGURE 12. The first (left) column: Inhomogeneous images with different levels of Gaussian noise: (0.01, 0.02, 0.03, 0.04); the second column: C-V method [25]; the third column: LBF method [43]; the fourth column: LIF method [20]; the fifth column: VLSBC method [34]; the sixth column: Zhang *et al.* method [35]; the seventh column: FRAGL [48]; the eighth column: proposed method.

figures contain the segmentation results of various methods over different Salt & Pepper noise levels: (0, 0.01, 0.02, 0.03, 0.04). The C-V [25] model performed well in Figs. 8 and 10,

and stuck in the local minima in Fig. 9. LBF [43] located the object boundaries but showed an inferior segmentation accuracy. Zhang *et al.* [35] fell in the local minima for

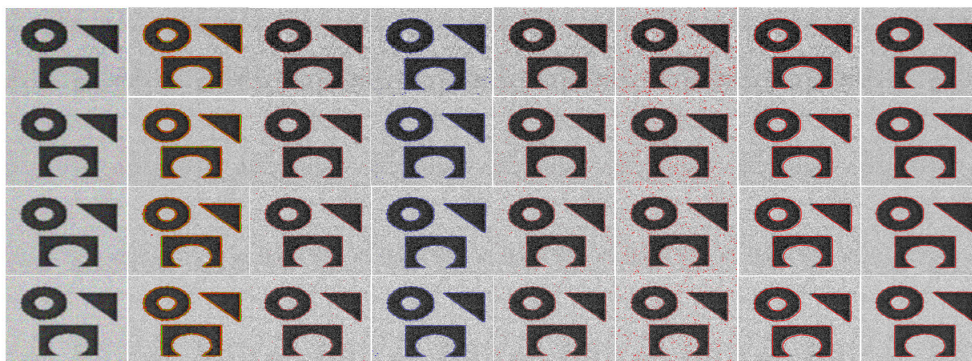


FIGURE 13. The first (left) column: Inhomogeneous images with different levels of Gaussian noise: (0.01, 0.02, 0.03, 0.04); the second column: C-V method [25]; the third column: LBF method [43]; the fourth column: LIF method [20]; the fifth column: VLSBC method [34]; the sixth column: Zhang et al. method [35]; the seventh column: FRAGL [48]; the eighth column: proposed method.

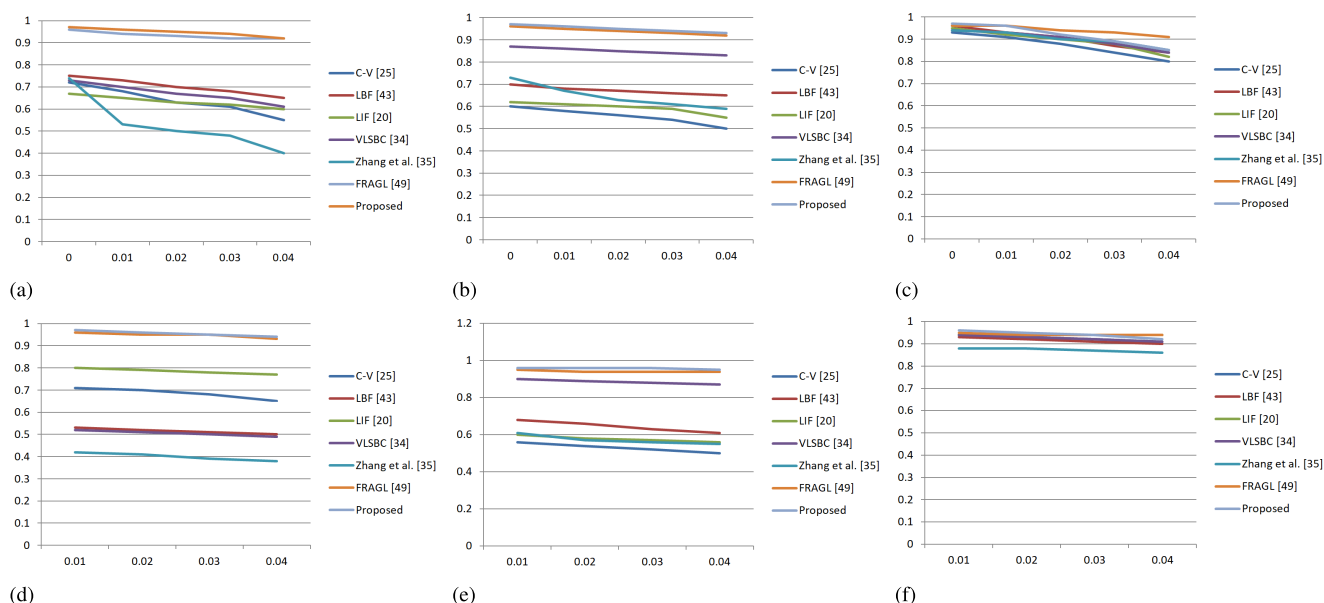


FIGURE 14. Jaccard Similarity (JS) values for Figs. 7, 8, 9, 10, 11 and 12 are represented by images a, b, c, d, e and f, respectively.

Figs. 8 and 9; however, it located the object boundaries in Fig. 10. The FRAGL [48] showed almost similar segmentation accuracy to the proposed model.

Figs. 11, 12 and 13 illustrate the segmentation results of three different images with different levels of Gaussian noise. From the top row to the fourth row of each of the figures contain the segmentation results of various methods over different Gaussian noise levels: (0.01, 0.02, 0.03, 0.04). In Fig. 12, the LBF [43] and VLSBC [34] models illustrated almost similar segmentation accuracy. FRAGL [48] attained outstanding performance, making it very near in segmentation accuracy to the proposed model. LIF [20] located the object boundaries, however, showed false contours in Fig. 11. The proposed method segmented ROIs with precision, irrespective of the image complexity, making it robust to noise. The respective accuracy charts of Figs. 8 to 13 are represented by images a, b, c, d, e and f in Fig. 14.

The proposed model has higher JS values compared to other state-of-the-art methods because of the proposed hybrid energy function. This section confirms that our model is robust to noise and can locate the exact object boundaries with a greater accuracy as compared to the previous methods.

B. QUANTITATIVE COMPARISON

A quantitative comparison of different models was performed to measure the Accuracy, Dice Index, and Sensitivity over mini-MIAS [45] database of mammograms. Furthermore, the segmentation results were compared with the respective ground truths. Fig. 15 presents the images taken from the mini-MIAS [45] database, their ground truths, and the result comparison of different methods with the proposed method, respectively. The obtained results are considered good if their values are closer to 1. The Accuracy, Dice Index, and Sensitivity metrics are defined

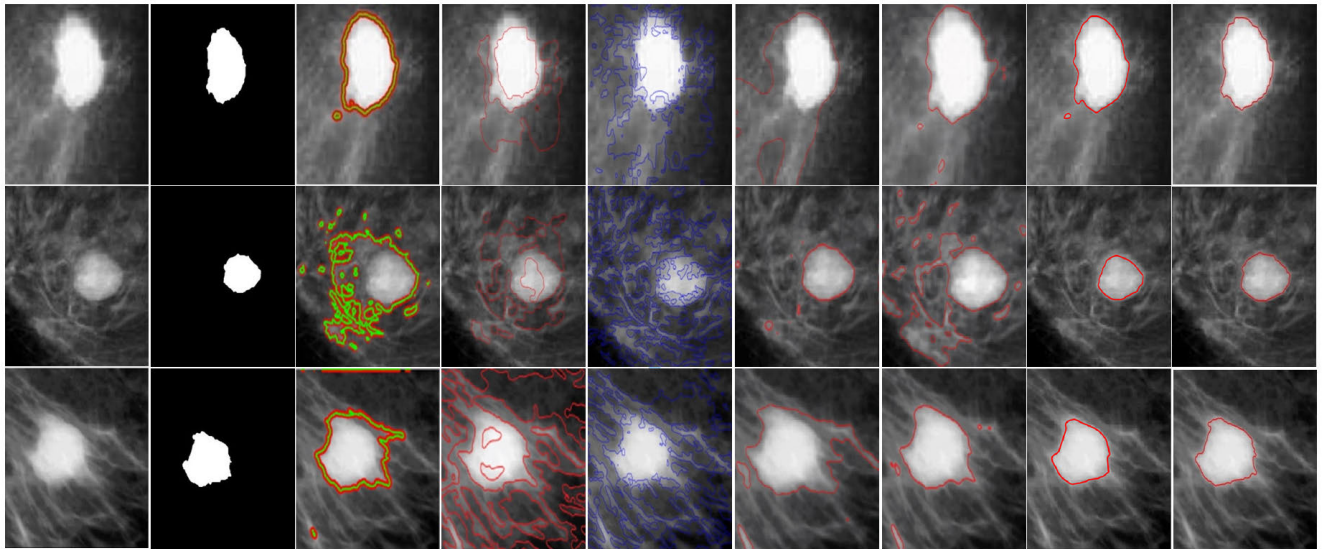


FIGURE 15. Proposed method on mammograms. First (left) column: Input image with different inhomogeneity levels; second column: C-V method [25]; third column: LBF method [43]; fourth column: LIF method [20]; fifth column: VLSBC method [34]; sixth column: Zhang et al. method [35]; seventh column: FRAGL method [49]; eighth column: Proposed method.

TABLE 4. CPU time and number of iterations required for segmentation results in Fig. 7.

Methods		Col 1	Col 2	Col 3
CV[25]	CPU Time (s)	18.9	12.05	7.01
	Iterations	500	500	500
LBF [43]	CPU Time (s)	15.17	12.78	8.21
	Iterations	500	500	500
LIF [20]	CPU Time (s)	8.18	6.42	3.09
	Iterations	500	500	500
VLSBC [34]	CPU Time (s)	13.17	6.57	3.53
	Iterations	78	50	50
Zhang et al. [35]	CPU Time (s)	6.78	8.78	5.37
	Iterations	13	17	11
FRAGL [48]	CPU Time (s)	5.74	2.81	2.41
	Iterations	80	30	60
Proposed Model	CPU Time (s)	5.36	2.78	2.08
	Iterations	8	7	5

as:

$$Accuracy = \frac{TP + TN}{TP + TN + FP + FN}, \quad (36)$$

$$DiceIndex = \frac{2 \times TP}{2 \times TP + FP + FN}, \quad (37)$$

and

$$Sensitivity = \frac{TP}{TP + FN}, \quad (38)$$

where Accuracy defines the closeness of the segmented regions to the actual regions, DSC is the dice coefficient to measure how much the detected region overlaps the actual regions, and Sensitivity defines that the detected region actually belongs to the actual region.

TP (true positive), TN (true negative), FP (false positive), and FN (false negative) correspond to the segmented

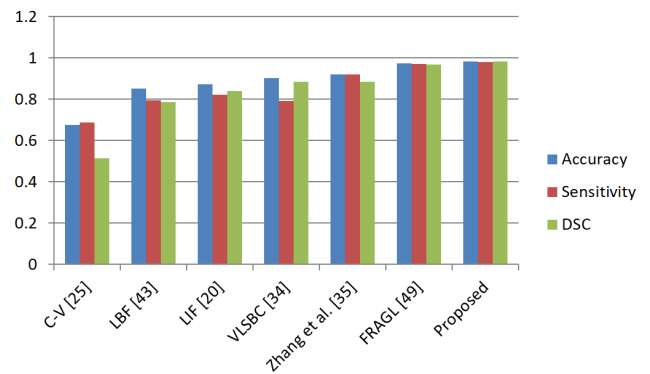


FIGURE 16. Metric analysis of the mammogram images.

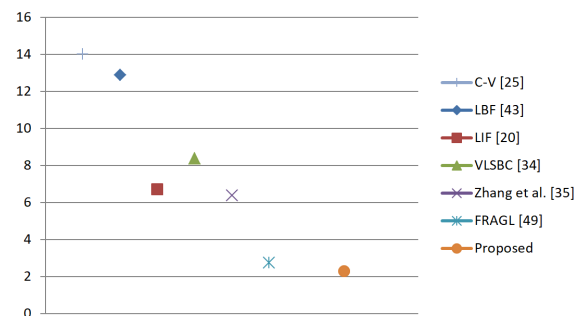


FIGURE 17. Graphical representation of average CPU time (s) for the segmentation of mammograms of [46].

actual-regions, correctly unsegmented regions, detected false-regions, and undetected actual-regions, respectively. The metric analysis of the mammogram images is shown in Fig. 16. We have also calculated the average CPU time (s) for the mini-MIAS database, as shown in Fig. 17.

Both techniques for the segmentation accuracy analysis confirm that the proposed hybrid energy model successfully

segments inhomogeneous images with greater CPU time (s) efficiency and accuracy.

VI. DISCUSSION

Previous level set methods are insufficient to segment images with inhomogeneous objects properly. The proposed ACM comprises advantageous features of both the previous local and global region-based methods. The performance of the proposed model is significantly superior to the other previous unsupervised ACM models in comparison. Deep learning image segmentation models efficiency relies on the training sample data set; with larger and more comprehensive data sets tending to produce better segmentation accuracy and efficiency. On comparatively small data sets, supervised learning tends to produce inferior results. However, unsupervised level set methods perform segmentation using pre-selected parameters depending on the ROI, whereas the proposed method sets the effective parameters in the new hybrid model to capture obscure regions in images.

VII. CONCLUSION

This paper proposes a hybrid energy function that comprises the local and global fitted models for the segmentation of intensity inhomogeneous images. The bias field is appended to the local fitted energy part in the proposed hybrid function to increase the effectiveness over inhomogeneous regions. Both the local and global energy functions are combined to strengthen each other's performance. Furthermore, the hybrid energy function is parametrized with weight coefficients to drag the contour accurately towards complex object-boundaries. The Gaussian filter is used to avoid re-initialization and to regularize the level set, whereas the new bias field initialization eliminates the contour initialization dependency. Noise sensitivity evaluation and the accuracy, dice index, and sensitivity metrics confirm the better performance of the proposed model over previous segmentation methods.

CONFLICT OF INTERESTS

The authors declare that there is no conflict of interests regarding the publication of this article.

REFERENCES

- [1] A. Elnakib, G. Gimel'farb, J. S. Suri, A. El-Baz, "Medical image segmentation: A brief survey," in *Multi Modality State-of-the-Art Medical Image Segmentation and Registration Methodologies*. New York, NY, USA: Springer, 2011, pp. 1–39.
- [2] R. Chakraborty, R. Sushil, and M. L. Garg, "An improved PSO-based multilevel image segmentation technique using minimum cross-entropy thresholding," *Arabian J. Sci. Eng.*, vol. 44, no. 4, pp. 3005–3020, Apr. 2019.
- [3] X. Zhang and S.-G. Zhao, "Cervical image classification based on image segmentation preprocessing and a CapsNet network model," *Int. J. Imag. Syst. Technol.*, vol. 29, no. 1, pp. 19–28, Mar. 2019.
- [4] S. Nishijima, K. Sugaya, K. Kadekawa, K. Ashitomi, T. Ueda, and H. Yamamoto, "Tadalafil improves bladder dysfunction and object recognition in rats with pelvic venous congestion," *Int. J. Urol.*, vol. 26, no. 5, pp. 578–585, May 2019.
- [5] E. Karami, M. S. Shehata, and A. Smith, "Adaptive polar active contour for segmentation and tracking in ultrasound videos," *IEEE Trans. Circuits Syst. Video Technol.*, vol. 29, no. 4, pp. 1209–1222, Apr. 2019.
- [6] M. Kass, A. Witkin, and D. Terzopoulos, "Snakes: Active contour models," *Int. J. Comput. Vis.*, vol. 1, no. 4, pp. 321–331, Jan. 1988.
- [7] S. Osher and J. A. Sethian, "Fronts propagating with curvature-dependent speed: Algorithms based on Hamilton–Jacobi formulations," *J. Comput. Phys.*, vol. 79, no. 1, pp. 12–49, Nov. 1988.
- [8] V. Caselles, F. Catté, T. Coll, and F. Dibos, "A geometric model for active contours in image processing," *Numerische Math.*, vol. 66, no. 1, pp. 1–31, Dec. 1993.
- [9] R. Goldenberg, R. Kimmel, E. Rivlin, and M. Rudzsky, "Fast geodesic active contours," *IEEE Trans. Image Process.*, vol. 10, no. 10, pp. 1467–1475, Oct. 2001.
- [10] C. Li, C. Xu, C. Gui, and M. D. Fox, "Distance regularized level set evolution and its application to image segmentation," *IEEE Trans. Image Process.*, vol. 19, no. 12, pp. 3243–3254, Dec. 2010.
- [11] C. Li, C. Xu, C. Gui, and M. D. Fox, "Level set evolution without re-initialization: A new variational formulation," in *Proc. IEEE Comput. Soc. Conf. Comput. Vis. Pattern Recognit. (CVPR)*, vol. 1, Jun. 2005, pp. 430–436.
- [12] V. Caselles, R. Kimmel, and G. Sapiro, "Geodesic active contours," *Int. J. Comput. Vis.*, vol. 22, no. 1, pp. 61–79, 1997.
- [13] B. Zhou and C.-L. Mu, "Level set evolution for boundary extraction based on a p-Laplace equation," *Appl. Math. Model.*, vol. 34, no. 12, pp. 3910–3916, Dec. 2010.
- [14] C. Huang and L. Zeng, "Level set evolution model for image segmentation based on variable exponent p-Laplace equation," *Appl. Math. Model.*, vol. 40, nos. 17–18, pp. 7739–7750, Sep. 2016.
- [15] Y. Wang and C. He, "Adaptive level set evolution starting with a constant function," *Appl. Math. Model.*, vol. 36, no. 7, pp. 3217–3228, Jul. 2012.
- [16] S. Lankton and A. Tannenbaum, "Localizing region-based active contours," *IEEE Trans. Image Process.*, vol. 17, no. 11, pp. 2029–2039, Nov. 2008.
- [17] L. Wang, Y. Chang, H. Wang, Z. Wu, J. Pu, and X. Yang, "An active contour model based on local fitted images for image segmentation," *Inf. Sci.*, vols. 418–419, pp. 61–73, Dec. 2017.
- [18] J. Miao, T.-Z. Huang, X. Zhou, Y. Wang, and J. Liu, "Image segmentation based on an active contour model of partial image restoration with local cosine fitting energy," *Inf. Sci.*, vol. 447, pp. 52–71, Jun. 2018.
- [19] C. Li, C.-Y. Kao, J. C. Gore, and Z. Ding, "Minimization of region-scalable fitting energy for image segmentation," *IEEE Trans. Image Process.*, vol. 17, no. 10, pp. 1940–1949, Oct. 2008.
- [20] K. Zhang, H. Song, and L. Zhang, "Active contours driven by local image fitting energy," *Pattern Recognit.*, vol. 43, no. 4, pp. 1199–1206, Apr. 2010.
- [21] X. Jiang, B. Li, Q. Wang, and P. Chen, "A novel active contour model driven by local and global intensity fitting energies," *Optik*, vol. 125, no. 21, pp. 6445–6449, Nov. 2014.
- [22] J. Oh, D. R. Martin, and X. Hu, "Partitioned edge-function-scaled region-based active contour (p-ESRAC): Automated liver segmentation in multiphase contrast-enhanced MRI," *Med. Phys.*, vol. 41, no. 4, Mar. 2014, Art. no. 041914.
- [23] S. Liu and Y. Peng, "A local region-based Chan–Vese model for image segmentation," *Pattern Recognit.*, vol. 45, no. 7, pp. 2769–2779, Jul. 2012.
- [24] H. Wang, T.-Z. Huang, Z. Xu, and Y. Wang, "An active contour model and its algorithms with local and global Gaussian distribution fitting energies," *Inf. Sci.*, vol. 263, pp. 43–59, Apr. 2014.
- [25] T. F. Chan and L. A. Vese, "Active contours without edges," *IEEE Trans. Image Process.*, vol. 10, no. 2, pp. 266–277, Feb. 2001.
- [26] S. Soomro, F. Akram, J. H. Kim, T. A. Soomro, and K. N. Choi, "Active contours using additive local and global intensity fitting models for intensity inhomogeneous image segmentation," *Comput. Math. Methods Med.*, vol. 2016, Sep. 2010, Art. no. 9675249.
- [27] S. Soomro, A. Munir, and K. N. Choi, "Hybrid two-stage active contour method with region and edge information for intensity inhomogeneous image segmentation," *PLoS ONE*, vol. 13, no. 1, Jan. 2018, Art. no. e0191827.
- [28] L. Wang, C. Li, Q. Sun, D. Xia, and C.-Y. Kao, "Active contours driven by local and global intensity fitting energy with application to brain MR image segmentation," *Comput. Med. Imag. Graph.*, vol. 33, no. 7, pp. 520–531, Oct. 2009.
- [29] A. Munir, S. Soomro, C. H. Lee, and K. N. Choi, "Adaptive active contours based on variable kernel with constant initialisation," *IET Image Process.*, vol. 12, no. 7, pp. 1117–1123, Jul. 2018.
- [30] S. Soomro, F. Akram, A. Munir, C. H. Lee, and K. N. Choi, "Segmentation of left and right ventricles in cardiac MRI using active contours," *Comput. Math. Methods Med.*, vol. 2017, pp. 1–16, Aug. 2017.

- [31] D. Mumford and J. Shah, "Optimal approximations by piecewise smooth functions and associated variational problems," *Commun. Pure Appl. Math.*, vol. 42, no. 5, pp. 577–685, Jul. 1989.
- [32] S. Ali and A. Madabhushi, "An integrated region-, boundary-, shape-based active contour for multiple object overlap resolution in histological imagery," *IEEE Trans. Med. Imag.*, vol. 31, no. 7, pp. 1448–1460, Jul. 2012.
- [33] C. Li, R. Huang, Z. Ding, J. C. Gatenby, D. N. Metaxas, and J. C. Gore, "A level set method for image segmentation in the presence of intensity inhomogeneities with application to MRI," *IEEE Trans. Image Process.*, vol. 20, no. 7, pp. 2007–2016, Jul. 2011.
- [34] K. Zhang, Q. Liu, H. Song, and X. Li, "A variational approach to simultaneous image segmentation and bias correction," *IEEE Trans. Cybern.*, vol. 45, no. 8, pp. 1426–1437, Aug. 2015.
- [35] K. Zhang, L. Zhang, K.-M. Lam, and D. Zhang, "A level set approach to image segmentation with intensity inhomogeneity," *IEEE Trans. Cybern.*, vol. 46, no. 2, pp. 546–557, Feb. 2016.
- [36] C. Li, J. C. Gore, and C. Davatzikos, "Multiplicative intrinsic component optimization (MICO) for MRI bias field estimation and tissue segmentation," *Magn. Reson. Imag.*, vol. 32, no. 7, pp. 913–923, Oct. 2018.
- [37] L. Wang, J. Zhu, M. Sheng, A. Cribb, S. Zhu, and J. Pu, "Simultaneous segmentation and bias field estimation using local fitted images," *Pattern Recognit.*, vol. 74, pp. 145–155, Feb. 2018.
- [38] B. Johnston, M. S. Atkins, B. Mackiewicz, and M. Anderson, "Segmentation of multiple sclerosis lesions in intensity corrected multispectral MRI," *IEEE Trans. Med. Imag.*, vol. 15, no. 2, pp. 154–169, Apr. 1996.
- [39] H. Min, L. Xia, J. Han, X. Wang, Q. Pan, H. Fu, H. Wang, S. T. C. Wong, and H. Li, "A multi-scale level set method based on local features for segmentation of images with intensity inhomogeneity," *Pattern Recognit.*, vol. 91, pp. 69–85, Jul. 2019.
- [40] D. Ma, Q. Liao, Z. Chen, R. Liao, and H. Ma, "Adaptive local-fitting-based active contour model for medical image segmentation," *Signal Process., Image Commun.*, vol. 76, pp. 201–213, Aug. 2019.
- [41] G. Huang, H. Ji, and W. Zhang, "A fast level set method for inhomogeneous image segmentation with adaptive scale parameter," *Magn. Reson. Imag.*, vol. 52, pp. 33–45, Oct. 2018.
- [42] G. Aubert and P. Kornprobst, *Mathematical Problems in Image Processing: Partial Differential Equations and the Calculus of Variations*, vol. 147. Berlin, Germany: Springer, 2006.
- [43] C. Li, C.-Y. Kao, J. C. Gore, and Z. Ding, "Implicit active contours driven by local binary fitting energy," in *Proc. IEEE Conf. Comput. Vis. Pattern Recognit. (CVPR)*, Jun. 2007, pp. 1–7.
- [44] C. Li, R. Huang, Z. Ding, C. Gatenby, D. Metaxas, and J. Gore, "A variational level set approach to segmentation and bias correction of images with intensity inhomogeneity," in *Proc. Int. Conf. Med. Image Comput. Comput. Assist. Intervent.* Berlin, Germany: Springer, 2008, pp. 1083–1091.
- [45] (2003). *The Mini-MIAS Database of Mammograms*. [Online]. Available: <http://peipa.essex.ac.uk/info/mias.html>
- [46] Y. Yu, C. Zhang, Y. Wei, and X. Li, "Active contour method combining local fitting energy and global fitting energy dynamically," in *Proc. Int. Conf. Med. Biometrics*. Berlin, Germany: Springer, 2010, pp. 163–172.
- [47] A. Tiwari, S. Srivastava, and M. Pant, "Brain tumor segmentation and classification from magnetic resonance images: Review of selected methods from 2014 to 2019," *Pattern Recognit. Lett.*, vol. 131, pp. 244–260, Mar. 2020.
- [48] J. Fang, H. Liu, L. Zhang, J. Liu, and H. Liu, "Fuzzy region-based active contours driven by weighting global and local fitting energy," *IEEE Access*, vol. 7, pp. 184518–184536, 2019.



ASIM NIAZ received the B.S. degree in electrical (computer) engineering from the COMSATS Institute of Information Technology, Pakistan, in 2016. He is currently pursuing the M.S. degree as a graduate Research Student with the Department of Computer Science and Engineering, Chung-Ang University, Seoul, South Korea.

Since 2018, he has been working as a Research Assistant with the Visual Image Media Laboratory, Chung-Ang University, under Prof. Dr. Choi. His current research interests include medical image analysis, semantic segmentation, and generative modeling.

KAYNAT RANA received the B.S. degree in electrical (computer) engineering from the COMSATS Institute of Information Technology, Pakistan, in 2016. She is currently pursuing the M.S. degree with the Department of Electrical Engineering, University of Engineering and Technology, Taxila, Pakistan. Since 2017, she has been working as a Lab Engineer (Junior Lecturer) with the Department of Computer Science and Engineering, HITEC University, Taxila. Her current research interests include medical image analysis, electronics, and generative modeling.



ADITI JOSHI received the B.S. degree in computer science and the M.B.A. degree in marketing from Mumbai University, India, in 2014 and 2016, respectively. She is currently pursuing the M.S. degree with the Department of Computer Science and Engineering, Chung-Ang University, Seoul, South Korea.

Since 2019, she has been working as a Research Assistant with the Visual Image Media Lab, Chung-Ang University, under Prof. Dr. Choi. Her current research interests include medical image analysis, semantic segmentation, and face and gesture recognition.



ASAD MUNIR received the bachelor's degree in engineering sciences from the GIK Institute, Pakistan, in 2013, and the master's degree in computer science from Chung-Ang University, South Korea, in 2018. He is currently pursuing the Ph.D. degree with the Department of Industrial and Information Engineering, Università degli Studi di Udine, Italy. His current research interests include object segmentation, object tracking, and person reidentification.



DAEUN DANA KIM received the bachelor's degree in computer science and engineering, in 2018, and the master's degree in application software from Chung-Ang University, South Korea. Her research fields are object detection and deep learning.



HYUN CHUL SONG received the B.S. and M.S. degrees in computer science from the Department of Computer Science, Chung-Ang University, Seoul, South Korea, in 2005 and 2007, respectively, and the Ph.D. degree in computer science with a major in application software from Chung-Ang University, in 2019. His research fields are object detection and deep learning.



KWANG NAM CHOI received the B.S. and M.S. degrees from the Department of Computer Science, Chung-Ang University, Seoul, South Korea, in 1988 and 1990, respectively, and the Ph.D. degree in computer science from the University of York, U.K., in 2002.

He is currently a Professor with the School of Computer Science and Engineering, Chung-Ang University. His current research interests include motion tracking, object categorization, and 3D image recognition.

...